Metal Ion Binding Properties and Conformational States of Calcium- and Integrin-Binding Protein†

Aaron P. Yamniuk, Leonard T. Nguyen, Tung T. Hoang, and Hans J. Vogel*

Structural Biology Research Group, Department of Biological Sciences, University of Calgary, 2500 University Drive Northwest, Calgary, Alberta, Canada T2N 1N4

Received August 11, 2003; Revised Manuscript Received January 16, 2004

ABSTRACT: Calcium- and integrin-binding protein (CIB) is a novel member of the helix−loop−helix family of regulatory calcium-binding proteins which likely has a specific function in hemostasis through its interaction with platelet integrin αIIbβ_3. The significant amino acid sequence homology between CIB and other regulatory calcium-binding proteins such as calmodulin, calcineurin B, and recoverin suggests that CIB may undergo a calcium-induced conformational change; however, the mechanism of calcium binding and the details of a structural change have not yet been investigated. Consequently, we have performed a variety of spectroscopic and microcalorimetric studies of CIB to determine its calcium binding characteristics, and the subsequent conformational changes that occur. Furthermore, we provide the first evidence for magnesium binding to CIB and determine the structural consequences of this interaction. Our results indicate that in the absence of any bound metal ions, apo-CIB adopts a folded yet highly flexible molten globule-like structure. Both calcium and magnesium binding induce conformational changes which stabilize both the secondary and tertiary structure of CIB, resulting in considerable increases in the thermal stability of the proteins. CIB was found to bind two Ca^{2+} ions in a sequential manner with dissociation constants (K_d) near 0.54 and 1.9 μM for sites EF-4 and EF-3, respectively. In contrast, CIB bound only one Mg^{2+} ion to EF-3 with a K_d near 120 μM. Together, our results suggest that CIB may exist in multiple structural and metal ion-bound states *in vivo* which may play a role in its regulation of target proteins such as platelet integrin.

CIB is a 191-amino acid intracellular protein that is constitutively expressed throughout the human body. The protein was discovered and named because of its interaction with the cytoplasmic domain of the αIIb subunit of platelet integrin αIIbβ_3, and its ability to specifically bind calcium (Ca^{2+}) (*1*). The high-affinity interaction with αIIb was originally detected through the use of the yeast two-hybrid system, and subsequently confirmed *in vitro* by surface plasmon resonance (*2*), isothermal titration calorimetry (ITC) (*3*), tryptophan fluorescence spectroscopy (*4*), and nuclear magnetic resonance (NMR) spectroscopy (A. P. Yamniuk and H. J. Vogel, unpublished observations). The binding of CIB to αIIbβ_3 has been demonstrated both *in vivo* and *in vitro* (*5*), and has been implicated as an important step in the integrin signaling events which includes important processes such as platelet aggregation during hemostasis (*6*). Moreover, several groups have identified a variety of other highly diverse target proteins that specifically interact with CIB, including those involved in neuronal function (Fnk and Snk kinase) (*7*−*9*), cell death (caspase-2S) (*10*), and Alzheimer's disease (Presenilin 2) (*11*) among others (*12*−*16*), suggesting that CIB may have several other functions in addition to the regulation of αIIbβ_3.

The sequence of CIB is highly homologous to the sequences of several members of the helix−loop−helix "EF-hand" Ca^{2+}-binding protein family, including calcineurin B (CnB), calmodulin (CaM), and recoverin. Like these proteins, CIB is predicted to contain four EF-hand calcium-binding motifs which likely fold into closely associated N- and C-terminal domains, more similar to the globular structure of CnB and members of the recoverin superfamily than the independent domains found in CaM (*4*, *17*). CIB has also been shown to bind Ca^{2+} (*1*), and although the stoichiometry of binding is unknown, it is only predicted to bind Ca^{2+} with its two C-domain EF-hands, EF-3 and -4. The two N-domain EF-hands of CIB, EF-1 and -2, are likely not functional due to the lack of many important Ca^{2+} coordinating residues as well as a large insertion in the middle of the Ca^{2+}-binding loop region of EF-1. This is in contrast to CnB and CaM, each of which contains four functional Ca^{2+}-binding sites (*18*, *19*), many of the recoverin homologues which can bind three Ca^{2+} ions (*20*−*23*), and recoverin which binds two Ca^{2+} ions to EF-2 and EF-3 (*24*, *25*). In addition, the N-terminal end of CIB was found to have a myristoylation consensus sequence, and like CnB, recoverin, and related proteins, it was demonstrated to be myristoylated and membrane-associated *in vivo* (*11*). However, it has also been shown that CIB can bind to αIIb independent of N-terminal

† This research is supported by the Canadian Institutes of Health Research (CIHR). H.J.V. holds a senior scientist award from the Alberta Heritage Foundation for Medical Research (AHFMR), while A.P.Y. is a recipient of AHFMR and National Sciences and Engineering Reseach Council of Canada (NSERC) studentship awards.

* To whom correspondence should be addressed. Phone: (403) 220-6006. Fax: (403) 289-9311. E-mail: vogel@ucalgary.ca.

10.1021/bi035432b CCC: $27.50
Published on Web 02/13/2004

Chart 1

```
ATGGGCCATCATCATCATCATCATCATCATCACAGCAGCGGCCATATCGACGACGAC
GACAAGCATATGGGCGGCAGCGGCAGCCGCCTGAGCAAAGAACTGCTGGCGGAATATCAG
GATCTGACCTTCCTGACGAAACAGGAAATCCTGCTGGCGCATCGTCGTTTTTGCGAACTG
CTGCCACAGGAACAGCGCAGCGTGGAAAGCAGCCTGCGCGCGCAGGTACCATTTGAACAG
ATCCTGAGCCTGCCAGAACTGAAAGCGAACCCATTTAAAGAACGCATCTGCCGCGTGTTT
AGCACCAGCCCAGCGAAAGATAGCCTGAGCTTTGAAGATTTTCTGGATCTGCTGAGCGTG
TTTAGCGATACCGCGACCCCAGATATCAAAAGCCATTATGCGTTTCGCATCTTTGATTTT
GATGATGATGGCACACTGAACCGCGAAGATCTGAGCCGCCTGGTGAACTGCCTGACAGGC
GAAGGCGAAGATACCCGCCTGAGCGCGAGCGAAATGAAACAGCTGATCGATAACATCCTG
GAAGAAAGCGATATCGATCGCGATGGTACCATCAACCTCAGCGAATTCCAGCATGTGATC
AGCCGCAGCCCAGATTTTGCGAGCAGCTTTAAAATCGTGCTGTGA
```

myristoylation, suggesting that unmyristoylated CIB is also a biologically active form of the protein (*5*).

In this study, we have used a variety of spectroscopic and calorimetric techniques to investigate the structure of CIB. In addition to studying the metal-free (apo-CIB) and Ca^{2+}-bound (Ca−CIB) conformations of the protein, we also studied the effects of Mg^{2+} on CIB (Mg−CIB). The latter is important since the Mg^{2+} concentration in the cell is in the millimolar range and might be sufficient to saturate the apoprotein in the absence of Ca^{2+}. In this work, we have studied the stoichiometry, thermodynamics, affinity, and mechanism of binding for both Ca^{2+} and Mg^{2+}. Our results demonstrate that apo-CIB has some secondary and tertiary structure, yet is likely very flexible. However, binding of both Ca^{2+} and Mg^{2+} to CIB provides considerable structural and thermal stability, increasing the α-helical content and decreasing the flexibility of the protein. Interestingly, we have identified EF-4 as a high-affinity Ca^{2+}-specific site, while EF-3 is a lower-affinity Ca^{2+}- and Mg^{2+}-binding site, which has a preference for Ca^{2+}.

MATERIALS AND METHODS

Protein Expression and Purification. CIB was expressed from a pET19b (Novagen) expression vector in *Escherichia coli* strain ER2566 from a synthetic gene designed with optimal *E. coli* codon usage. The final gene sequence includes a 10-His tag and enterokinase cleavage site (Chart 1).

The gene was constructed from overlapping coding and noncoding oligonucleotides of ∼75 bases each, which were filled by PCR. Any errors that were introduced were corrected by site-directed mutagenesis.

For expression of CIB, 1.0 L of Luria-Bertani (LB) broth containing 100 mg/L ampicillin was inoculated with approximately 10 mL of overnight culture in the same medium, and grown at 37 °C to an OD_{600} of ∼0.8. Expression of CIB was induced by the addition of 100 mg of IPTG/L of culture, and the mixture was incubated in a shaker at 37 °C for 4 h or at room temperature for 8 h. Cells were harvested by centrifugation, flash-frozen, and stored at −80 °C. Frozen cell pellets were resuspended in 20 mM HEPES, 500 mM NaCl (pH 7.9), and 1.6 mg/mL PMSF, homogenized, and then French pressed between three and six times at 14 000 psi. Cell debris was removed by centrifugation, and the resulting supernatant was filtered before being loaded on a chelating Sepharose fast flow column (Amersham Pharmacia) pre-equilibrated with 100 mM $NiSO_4$ and then 20 mM HEPES and 500 mM NaCl (pH 7.9). Contaminating proteins and DNA were removed by washing the column with 20 mM HEPES, 500 mM NaCl, and 100 mM imidazole (pH 7.9), and CIB was then eluted sharply in 20 mM HEPES, 500 mM NaCl, and 500 mM imidazole (pH 7.9). Fractions containing CIB were subsequently diluted six times with 20 mM HEPES (pH 7.5), to lower the ionic strength, and loaded onto a DEAE anion exchange column equilibrated with 20 mM HEPES (pH 7.5). This column was washed with 20 mM HEPES and 100 mM NaCl (pH 7.5) to remove remaining contaminants, and pure CIB was sharply eluted in 20 mM HEPES and 500 mM NaCl (pH 7.9). Fractions containing CIB were pooled and dialyzed over the course of 48 h in several changes of 8 mM NH_4HCO_3 (pH 7.0) before lyophilization. Typical yields were between 30 and 50 mg of pure CIB/L of culture. Uniformly ^{15}N-labeled CIB ([^{15}N]CIB) was expressed and purified in a manner similar to that of the unlabeled protein, except that only 5 mL of overnight preculture in LB broth was used to inoculate 1.0 L of M9 minimal medium, containing 1 g/L $^{15}NH_4Cl$ and 100 mg/L ampicillin. Concentrations of CIB were determined by UV spectroscopy ($\epsilon_{276} = 2900\ M^{-1}\ cm^{-1}$), or using the Bio-Rad protein assay kit.

Preparation of Apo-, Mg−, and Ca−CIB. To prepare samples of apo-, Ca−, and Mg−CIB for CD, DSC, NMR, and fluorescence spectroscopy studies, we used various combinations of $CaCl_2$, $MgCl_2$, the high-affinity Ca^{2+} and Mg^{2+} chelator EDTA, and the Ca^{2+}-specific chelator EGTA. Since the metal ion binding affinity of EDTA and EGTA varies with conditions such as temperature, pH, and ionic strength, we determined the dissociation constants for the interaction of both Ca^{2+} and Mg^{2+} with either EDTA or EGTA under our experimental conditions using ITC. In 20 mM HEPES and 100 mM KCl (pH 7.4) at 30 °C, we obtained the following K_d values: 95 nM for Ca^{2+}−EDTA, 1.4 μM for Mg^{2+}−EDTA, 25 nM for Ca^{2+}−EGTA, and 4.6 mM for Mg^{2+}−EGTA. Because we were unable to prepare

totally calcium-deficient apo-CIB by treatment with Chelex-100 (Bio-Rad), samples of apo-CIB contained some EDTA, or EDTA and EGTA, Mg−CIB samples contained EGTA to bind residual Ca^{2+}, as well as excess Mg^{2+} to bind to the protein, while samples of Ca−CIB simply contained an excess of Ca^{2+}. ^{1}H NMR spectroscopy studies demonstrated that titration of Ca^{2+} or Mg^{2+} into samples containing an excess of EDTA resulted in no shifting of the CIB protein peaks until after the EDTA was completely saturated with the respective metal ion, suggesting that CIB was completely metal-free in the presence of EDTA. There is also no evidence that either EDTA or EGTA binds to CIB, and each is easily removed by dialysis or gel filtration chromatography.

Circular Dichroism (CD) Spectroscopy. CD spectra were recorded at room temperature on a Jasco J-715 spectropolarimeter in the Department of Chemistry of the University of Calgary. All far-UV CD spectra were recorded in a cylindrical quartz cuvette with a path length of 0.1 cm, and a volume of 300 μL, on samples consisting of 10 μM CIB in 5 mM HEPES, 0.5 mM DTT (pH 7.5), and either 2 mM $CaCl_2$ for Ca−CIB samples, 2 mM $MgCl_2$ and 0.5 mM EGTA for Mg−CIB samples, or 1 mM EDTA and 1 mM EGTA for apo-CIB samples. Spectra were recorded from 260 to 185 nm using the following parameters: step resolution of 0.2 nm, speed of 100 nm/min, response time of 2.0 s, bandwidth of 1.0 nm, and a sensitivity of 20 mdeg. All far-UV spectra are the average of 10 scans with the background signal from the buffer subtracted, and the data were smoothed and converted to molar ellipticity using Jasco software. Near-UV spectra were recorded in a 1.0 cm path length cylindrical quartz cuvette with a volume of 2.0 mL on samples of 65 μM CIB in 20 mM HEPES, 100 mM KCl, 5 mM DTT, and the same Ca, Mg, EDTA, and EGTA concentrations that were used for the far-UV samples. These spectra are the average of 20 scans, which were not smoothed so that the fine structure of the spectra could be maintained. All other parameters were identical to those for the far-UV samples except that the sensitivity was set to 10 mdeg.

Fluorescence Spectroscopy. 8-Anilino-1-naphthalenesulfonate (ANS) fluorescence spectroscopy studies were performed on samples of 30 μM CIB in 20 mM HEPES, 100 mM KCl, 1 mM DTT, 120 μM ANS (pH 7.5), and either 2 mM EDTA and 2 mM EGTA for apo-CIB, 2 mM $CaCl_2$ for Ca−CIB, or 2 mM $MgCl_2$ and 0.5 mM EGTA for Mg−CIB. All spectra were recorded from 400 to 600 nm using excitation and emission bandwidths of 5 and 10 nm, respectively, on a Varian Cary Eclipse spectrofluorimeter at 37 °C.

Differential Scanning Calorimetry (DSC). To prepare the CIB samples for DSC, lyophilized CIB was dissolved in 20 mM HEPES and 10 mM DTT (pH 7.5) to a concentration of 300−450 μM, and then incubated at room temperature for approximately 20 h to reduce any disulfide bonds. DTT was removed by passing the samples through a Bio-Rad 10 DG column equilibrated with 20 mM HEPES and 100 mM KCl (pH 7.5) immediately prior to carrying out each experiment. The protein was then diluted with 20 mM HEPES and 100 mM KCl (pH 7.5), and $CaCl_2$, $MgCl_2$, EDTA, or EGTA was added from a concentrated stock solution to give 2 mM $CaCl_2$ for Ca−CIB, 2.5 mM EDTA and 2.5 mM EGTA for apo-CIB, and 4 mM $MgCl_2$ and 1 mM EGTA for Mg−CIB. Alternatively, CIB was dialyzed against 20 mM HEPES, 100 mM KCl, and 1 mM β-mercaptoethanol (βME) for a minimum of 24 h at room temperature and then diluted to appropriate concentrations with dialysis buffer and used directly for DSC studies. Results in the presence of βME were similar to those obtained using the desalting method, although baselines were less stable due to the presence of βME. All samples were centrifuged prior to carrying out the experiment and examined for precipitates, but none were observed in any of the apo-, Ca−, or Mg−CIB samples. Samples of 25−175 μM CIB were heated in a MicroCal VP-DSC microcalorimeter from 10 to 110 °C at a scan rate of 60 K/h, and then cooled and rescanned to check for the reversibility of the thermal transitions. The pressure was maintained above 28 psi to prevent degassing of the samples at higher temperatures. Scans were performed with CIB in the sample cell and the respective buffer in the reference cell, and a buffer−buffer scan was subtracted in each case to correct for instrument baselines. Data analysis for all experiments was performed using MicroCal Origin software.

Isothermal Titration Calorimetry (ITC). Samples for ITC were prepared in essentially the same manner as those for DSC involving DTT incubation and desalting. Additionally, we passed the DTT-free samples through Calcium Sponge S (Molecular Probes) column equilibrated with 20 mM HEPES and 100 mM KCl (pH 7.4) to remove Ca^{2+} ions. All buffers were prepared in acid-washed plastic containers using ultrapure MilliQ water and stripped of metal ions by dialyzing for several days with a dialysis bag filled with Chelex-100 (Bio-Rad). ITC experiments were performed on a MicroCal VP-ITC microcalorimeter at 30 °C and analyzed using MicroCal Origin software. Each titration consisted of 3−5 μL injections of concentrated $CaCl_2$ or $MgCl_2$ in 20 mM HEPES and 100 mM KCl (pH 7.4) into a 1.43 mL sample cell containing 100−150 μM CIB in a similar buffer with and without 2 mM $CaCl_2$ or $MgCl_2$. For each titration, the stoichiometry (N), association constant (K_a), and enthalpy change (ΔH) were directly obtained from the ITC data while the dissociation constant (K_d) was calculated as $1/K_a$.

NMR Spectroscopy. All ^{1}H−^{15}N HSQC NMR spectra were recorded at 37 °C on a Bruker Avance 500 NMR spectrometer equipped with a triple-resonance inverse cryoprobe with a single axis z-gradient. Each spectrum was acquired with quadrature detection in the F_1 dimension obtained using the echo/antiecho time-proportional phase increment method. The 1024 × 64 real data matrix was zero-filled once in each dimension. For the titration of apo-CIB with Ca^{2+}, a 480 μL sample containing 620 μM uniformly ^{15}N-labeled CIB, 100 mM KCl, 10 mM DTT, and 10% D_2O (pH 7.5 ± 0.1) containing 1 mM EDTA was titrated with microliter additions of concentrated $CaCl_2$ in H_2O. For the titration of apo-CIB with Mg^{2+}, a 440 μL sample containing 565 μM uniformly ^{15}N-labeled CIB, 100 mM KCl, 10 mM DTT, and 10% D_2O (pH 7.5 ± 0.1) containing 1 mM EDTA and 0.30 mM EGTA was titrated with microliter additions of concentrated $MgCl_2$ and then $CaCl_2$ in H_2O. The pH was kept at all times within 0.1 pH unit with small additions of concentrated NaOH. The proton chemical shifts were referenced to 0 ppm using the DSS (2,2-dimethyl-2-silapentane-5-sulfonate) signal in the one-dimensional ^{1}H spectrum of each sample, and then ^{15}N chemical shifts were referenced indirectly to DSS using a

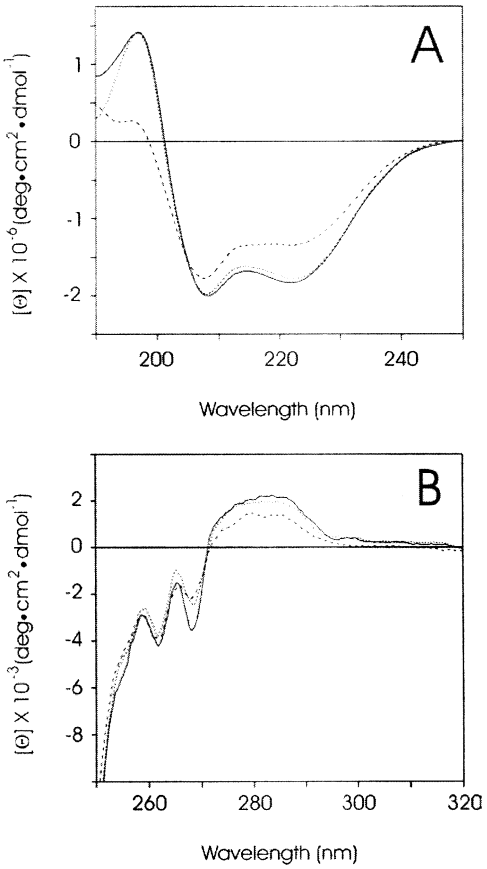

FIGURE 1: Circular dichroism spectra of apo-CIB (- - -), Ca−CIB (—), and Mg−CIB (•••), recorded at room temperature: (A) far-UV spectra of 10 μM CIB and (B) near-UV CD spectra of 65 μM CIB.

conversion factor of 0.101 329 118 as suggested by Sykes and co-workers (*26*).

RESULTS

Circular Dichroism Spectroscopy. To investigate the secondary structure of CIB in the apo and Ca- and Mg-bound states, we performed far-UV CD spectroscopy at room temperature. The intense negative ellipticity near 208 and 222 nm in the spectrum of apo-CIB indicates that the protein has significant α-helical character (Figure 1A). However, the small amplitude of the positive 196 nm band, and considerably greater intensity of the 208 nm band in comparison to that of the 222 nm band, suggest that apo-CIB also has a significant proportion of random coil structure, or regions of high flexibility (*27*). In the presence of both Ca^{2+} and Mg^{2+}, we observed considerable increases in the intensity of each of the 196, 208, and 222 nm bands, suggesting that CIB specifically binds to both Ca^{2+} and Mg^{2+} and that the binding of each ion induces conformational changes which increase the amount of stable α-helical secondary structure in the protein. In comparison to the apo-CIB spectrum, the intensities of the 222 nm bands of Ca− and Mg−CIB increase by 36.0 and 32.1%, respectively, in comparison to increases of only 13.4 and 11.9% for the 208 nm bands, respectively, suggesting that in addition to an increased α-helical content both Ca− and Mg−CIB experience a decrease in unstructured or flexible regions compared to apo-CIB.

Near-UV CD spectroscopy is commonly used to study the environment of the aromatic amino acid side chains, where

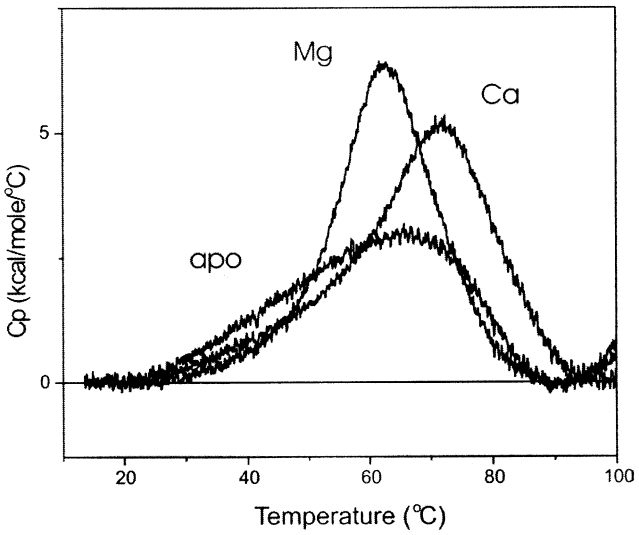

FIGURE 2: Baseline-corrected and concentration-normalized DSC thermograms for 100 μM samples of apo-, Ca−, and Mg−CIB, recorded at a scan rate of 60 K/h.

the shape and intensity of the CD signals are very sensitive to the side chain's precise environment (*28*). CIB contains a total of 14 Phe residues and two Tyr residues which combine to produce the near-UV CD spectrum of the protein. The strong positive Tyr signals from ~270−295 nm and the negative Phe signals below 270 nm indicate that CIB has a significant amount of tertiary structure in the Ca^{2+}- and Mg^{2+}-bound states as well as in the absence of any bound metal ions (Figure 1B). However, like the far-UV CD spectra, the signal intensity for apo-CIB is considerably smaller than that for either Ca− or Mg−CIB, suggesting that apo-CIB has a distinct tertiary structure. Although the signal intensities of Ca−CIB and Mg−CIB are similar, Ca−CIB consistently produced slightly more intense signals in both near- and far-UV spectra, suggesting that CIB adopts a slightly more stable structure when bound to Ca^{2+}.

Differential Scanning Calorimetry. Since the CD spectroscopy data suggested that Ca^{2+} and Mg^{2+} binding to CIB each had a stabilizing effect on the secondary and tertiary structure of the protein, with Ca^{2+} having a slightly more pronounced effect, we anticipated that a similar trend might be observed in the thermal stability of the protein. To test this hypothesis, we performed DSC studies on apo-, Ca−, and Mg−CIB at several different protein concentrations ranging from 25 to 175 μM. The best results were obtained using 100 μM apo-, Ca−, and Mg−CIB, and these baseline-corrected and concentration-normalized spectra are overlaid in Figure 2. Interestingly, in the DSC thermogram for apo-CIB, we observed a very broad thermal transition beginning near 25 °C with no obvious single transition peak, suggesting that apo-CIB may slowly unfold through several intermediate steps beginning at low temperatures. In contrast, Mg−CIB displayed a single sharp transition peak indicating that CIB likely unfolds as a single cooperative unit when bound to Mg^{2+}. The thermogram for Ca−CIB also displayed one major thermal transition peak, although a minor peak was also detected near 45−50 °C. Consistent with homology modeling studies, this suggests that the two predicted domains of CIB are closely associated with each other (*4*, *17*). Unfortunately, apo-, Ca−, and Mg−CIB each produced negative and nonlinear post-transition baselines independent

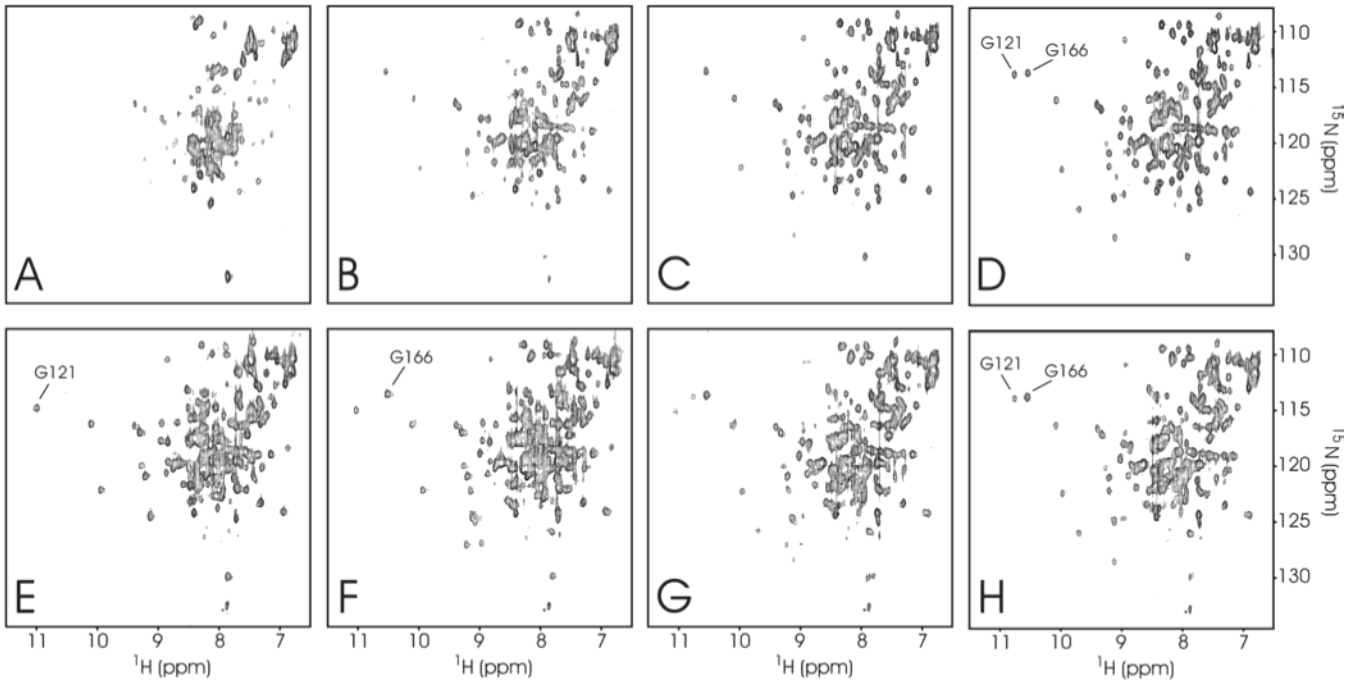

FIGURE 3: $^{1}H-^{15}N$ HSQC NMR spectra of [^{15}N]apo-CIB in the presence of (A) 0, (B) 0.5, (C) 1.0, and (D) 2.0 molar equiv of Ca^{2+} and spectra of [^{15}N]Mg−CIB in the presence of approximately (E) 0, (F) 1.0, (G) 1.5, and (H) 2.0 molar equiv of bound Ca^{2+}. Spectra E−H were recorded in the presence of 6.4 molar equiv of Mg^{2+}. Note the sequential filling of EF-4 and then EF-3 as monitored by the appearance of Gly166 and then Gly121 in each row (see the text).

of concentration, a characteristic highly suggestive of aggregation. Furthermore, rescanning the samples after cooling revealed no endothermic transition peaks, indicating that CIB likely could not dissociate and refold from the aggregated state (results not shown). Because of this aggregation, the post-transition baselines could not be accurately defined, and as a result, the calorimetric enthalpy (ΔH_c) and van't Hoff enthalpy (ΔH_v) were not calculated. The combination of this aggregation and the gradualness of the apo-CIB denaturation thermogram also made the determination of an accurate melting temperature impossible for apo-CIB. However, the transition temperatures (T_m) for Ca− and Mg−CIB were determined to be accurate to ±1.5 °C at all concentrations between 25 and 100 μM independent of how the baselines were defined. Concentrations greater than 100 μM CIB showed extreme exothermic aggregation effects, leading to inaccurate T_m determination. The T_m value for Ca−CIB (72.1 °C) in comparison to that of Mg−CIB (62.8 °C) in the 100 μM samples demonstrates that binding of Ca^{2+} to CIB induces an approximately 10 °C stability increase over that of the Mg^{2+}-bound protein. Therefore, the thermal stability analysis of CIB is consistent with the CD spectroscopy data, suggesting that both Mg^{2+} and Ca^{2+} have a stabilizing effect on the structure of apo-CIB, with Ca^{2+} providing greater structural stability. Furthermore, the results show that apo-CIB is likely highly flexible and in a partially disordered state near-physiological temperatures.

NMR Spectroscopy. To obtain a more detailed view of the Ca^{2+}- and Mg^{2+}-induced conformational changes in CIB, we performed heteronuclear $^{1}H-^{15}N$ HSQC (heteronuclear single-quantum coherence) NMR spectroscopy studies of uniformly ^{15}N-labeled CIB ([^{15}N]CIB). This technique is useful for monitoring the amide backbone in investigating the protein structure and global conformational changes. All experiments were performed under near-physiological conditions of temperature (37 °C), pH (7.5 ± 0.1), and ionic strength (100 mM KCl), in a highly reducing environment (10 mM DTT) to keep CIB in a native-like conformation. Titrations of either Ca^{2+} or Mg^{2+} into apo-CIB were performed individually to monitor the structural consequences of binding each ion, as well as a titration of Ca^{2+} into Mg-saturated CIB to investigate possible competition between the two ions.

In the initial HSQC spectrum of apo-CIB recorded in the presence of a molar excess of EDTA, we found a lack of chemical shift dispersion, broad line widths, and clustering of many of the peaks around typical random coil values suggestive of a high degree of flexibility (Figure 3A). However, several of the backbone amide resonances were observed to have unique chemical shifts with sharper line widths, indicating that some regions of apo-CIB had well-defined structure. Because the CD spectra indicated that apo-CIB had considerable secondary and tertiary structure, the characteristics observed in the NMR spectrum of apo-CIB suggest that the protein is likely highly flexible and possibly in a molten globule type of conformation. The broad thermal transition for apo-CIB seen in our DSC results is also consistent with a flexible molten globule type of structure. It is interesting to note that several other small regulatory Ca^{2+}-binding proteins have strikingly similar NMR spectra in the absence of Ca^{2+}, including Frq1 (*21*), GCAP-2 (*20*), and calerythrin (*29*), suggesting that these characteristics are not unique to apo-CIB, and may represent a common conformational state for many related Ca^{2+}-binding proteins in the absence of Ca^{2+}.

During the Ca^{2+} titration, we observed no shifting of any of the apo-CIB peaks until after the EDTA was completely saturated with Ca^{2+}, indicating that under these experimental conditions CIB has an at least 10-fold lower affinity for Ca^{2+} than EDTA, as there is little competition between them

(results not shown). However, as the first equivalent of Ca^{2+} binds to CIB we observe a complete disappearance of all of the apo-CIB peaks and now detect an entire new significantly more disperse set of resonances characteristic of a well-folded protein (Figure 3B,C). This suggests that CIB binds the first equivalent of Ca^{2+} with a relatively high affinity since the protein is in slow chemical exchange between Ca^{2+}-bound and unbound conformations. Furthermore, it is evidence of a significant Ca^{2+}-induced conformational change and stabilization of secondary and tertiary structure. Titration of the second equivalent of Ca^{2+} results in the detection of a small number of additional peaks, suggesting that a comparably minor conformational change occurs upon binding this second Ca^{2+} equivalent (Figure 3D). Further titration of Ca^{2+} produced no significant changes in the spectra, confirming the predicted number of two functional Ca^{2+}-binding sites in CIB. Worth noting is the fact that we detected fewer peaks in all $^1H-^{15}N$ HSQC spectra of [^{15}N]CIB than we expected. While this can in part be attributed to a combination of peak overlap and chemical exchange, both dynamic light scattering (DLS) and small-angle X-ray scattering (SAXS) studies suggest that protein aggregation may also contribute to peak broadening in all states of CIB (results not shown). No significant improvements in the NMR spectra of apo-, Ca−, or Mg−CIB could be obtained by varying the protein concentration, temperature, pH, or ionic strength or by the addition of various detergents to the samples.

In the sample of apo-CIB used for titration with Mg^{2+}, we included the Ca^{2+}-specific chelator EGTA in addition to the Ca^{2+} and Mg^{2+} chelator EDTA as described in Materials and Methods. As expected, the apo-CIB resonances were unaffected by titration with Mg^{2+} until after complete saturation of the EDTA (results not shown). Then as Mg^{2+} bound to the protein a new set of peaks arising from Mg−CIB were observed in slow exchange with the apo-CIB peaks (Figure 3E). The number of detected peaks and the spectral dispersion of the Mg−CIB spectra are similar to those of Ca−CIB, although fewer well-resolved peaks are detected, and a cluster of residues likely with high flexibility still exists in the center of the spectrum as in apo-CIB. This suggests that although the structure of Mg−CIB is quite similar to that of Ca−CIB, overall Mg−CIB is somewhat more flexible, an observation consistent with our CD and DSC studies. It was surprising to find that the majority of the well-resolved peaks in the Mg−CIB spectra had chemical shifts that were identical to those of peaks in the spectrum of Ca^{2+}-saturated CIB, which suggests that several regions of Ca− and Mg−CIB have similar conformations. As we titrated Ca^{2+} into the Mg−CIB sample, several of the peaks were observed to shift, producing a spectrum nearly identical to that of Ca−CIB in the absence of Mg^{2+}, suggesting that CIB binds Ca^{2+} with a considerably higher affinity than Mg^{2+} (Figure 3F−H). Of note is the fact that the two spectra are not completely identical, suggesting that Mg^{2+} may have a minor effect on other regions of the protein as well.

One area that differs between the spectra of Ca− and Mg−CIB is that between 11.3 and 10.2 ppm in the ^1H dimension and between 112 and 117 ppm in the ^{15}N dimension, which contains peaks with chemical shifts characteristic of the invariant Gly residues at position 6 of nearly all functional Ca^{2+}-binding loops. In EF-3 and EF-4 of CIB, these residues correspond to Gly121 and -166, respectively, as seen in the 12-residue Ca^{2+}-binding loop sequences of CIB shown below, where the asterisks represent the Ca^{2+}-coordinating residues.

```
          * * * * *  *

116   DFDDDGTLNRED

161   DIDRDGTINLSE
```

We have assigned these Gly residues by three-dimensional NMR spectroscopy of ^{13}C- and ^{15}N-labeled Ca−CIB, and confirmed that these resonances arise from Gly residues by $^1H-^{15}N$ HSQC NMR spectroscopy of CIB specifically labeled with [^{15}N]Gly (results not shown). The identities of these two Gly residues are indicated in Figure 3. Interestingly, when we titrated the first equivalent of Ca^{2+} into apo-CIB, only Gly166 was detected, indicating that most of the Ca^{2+} is bound to only EF-4 (Figure 3B,C). Titration of the second Ca^{2+} equivalent has very little effect on the intensity and chemical shift of first Gly peak, but we now observe an increase in the intensity of Gly121 in EF-3 (Figure 3D). Together, these results suggest that unlike many EF-hand pairs such as those in CaM which bind Ca^{2+} cooperatively, the EF-hand pair of CIB binds Ca^{2+} in a sequential manner.

In contrast to the spectrum of Ca−CIB, the Mg−CIB spectrum shows only one Gly residue even in the presence of excess Mg^{2+}, suggesting that CIB binds only 1 molar equiv of Mg^{2+}. As might be expected due to the different Ca^{2+}- and Mg^{2+}-bound loop conformations found in EF-hand motifs, this peak also had a slightly different chemical shift in both the ^1H and ^{15}N dimensions than either of the Gly residues in Ca−CIB. Interestingly, as Ca^{2+} was titrated into the sample of Mg−CIB, we initially observed only Gly166 while the Gly peak at the Mg^{2+}-bound site remained unaffected. Further titration of Ca^{2+} resulted in the appearance of Gly121 with the corresponding disappearance of the Mg-bound Gly peak (Figure 3F−H). This suggests that the Gly peak in the Mg−CIB spectrum arises from Gly121 and that the bound Mg^{2+} is exchanged for Ca^{2+} during the titration. Together, these results propose that EF-3 of CIB is a lower-affinity Ca^{2+}- and Mg^{2+}-binding site with a preference for Ca^{2+}, while EF-4 is a higher-affinity Ca^{2+}-specific site. Furthermore, Ca^{2+} binding remains a sequential process even in the presence of Mg^{2+}.

Isothermal Titration Calorimetry. To better characterize the Ca^{2+} and Mg^{2+} binding behavior of CIB, we performed various ITC titrations of the protein at 30 °C. Titration of Ca^{2+} into apo-CIB produced a binding curve consisting of two sequential sigmoidal curves, indicating that the protein bound two Ca^{2+} ions in a sequential manner, consistent with the sequential binding to EF-4 and then EF-3 observed in our NMR data (Figure 4). The calculated dissociation constant (K_d) for binding to EF-4 (0.54 ± 0.07 μM) was ~3.5 times greater than that for binding to EF-3 (1.9 ± 0.3 μM), suggesting that despite it being a sequential process, the binding curves overlap somewhat (Table 1). The affinity of EF-4 is also ~1 order of magnitude smaller than the Ca^{2+} affinity of EDTA under these conditions (see Materials and Methods and ref *30*), as predicted by our NMR results. The low stoichiometry (N) of binding to EF-4 (0.28 ± 0.04) is attributed partly to the overlapping binding curves, but also

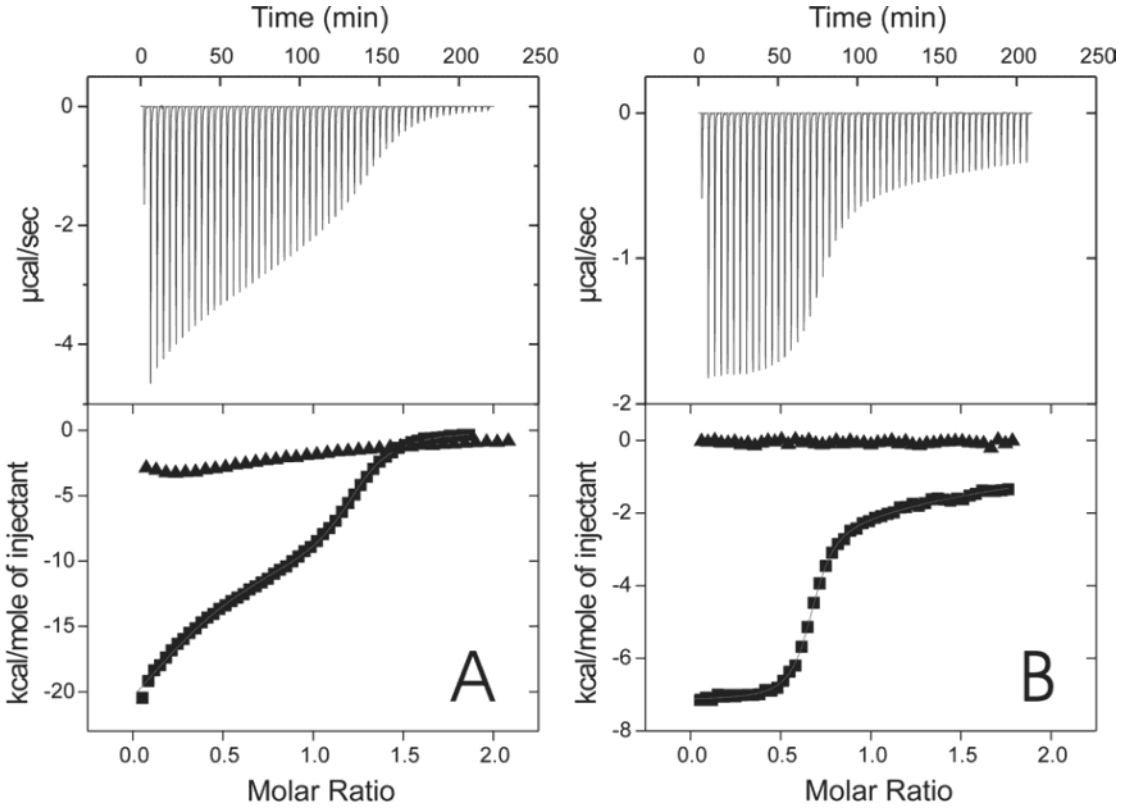

FIGURE 4: (A) ITC calorimetric trace for the titration of apo-CIB with Ca^{2+} (top) and the derived binding isotherm for the titration of apo-CIB with Ca^{2+} (■) and Mg^{2+} (▲) demonstrating the considerably larger heat released upon binding Ca^{2+} (bottom). (B) ITC calorimetric trace for the titration of Mg−CIB with Ca^{2+} (top) and the derived binding isotherm for the titration of Mg−CIB with Ca^{2+} (■) and Ca−CIB with Mg^{2+} (▲) (bottom). All experiments were performed at 30 °C.

Table 1: Thermodynamic Parameters for Titrations of CIB with Ca^{2+} or Mg^{2+} in 20 mM HEPES and 100 mM KCl (pH 7.4)[a]

	EF-4			EF-3		
experiment	*N*	K_d (μM)	ΔH (kcal/mol)	*N*	K_d (μM)	ΔH (kcal/mol)
binding of Ca^{2+} to apo-CIB	0.28 ± 0.04	0.54 ± 0.07	−32.4 ± 6.91	0.94 ± 0.05	1.9 ± 0.3	−6.22 ± 1.22
binding of Mg^{2+} to apo-CIB				0.81 ± 0.04	120 ± 5.0	−8.64 ± 0.49
binding of Ca^{2+} to Mg−CIB	0.66 ± 0.00	0.48 ± 0.03	−7.16 ± 0.02	1.0[b]	198 ± 20	−6.29 ± 0.34
binding of Mg^{2+} to Ca−CIB[c]				–	–	–

[a] All experiments were performed at 30 °C. The values for stoichiometry (*N*), dissociation constant (K_d), and enthalpy change (ΔH) for each binding event are shown. [b] This value was fixed during the fitting procedure due to low affinity. [c] Essentially no binding (see the text).

likely to some residual Ca^{2+} contamination, while the *N* for EF-3 was near the expected 1.0 molar equiv (Table 1). As seen in Figure 4, binding of Ca^{2+} to CIB proceeds with a large negative enthalpy change (ΔH), indicating that it is a highly exothermic interaction. In ITC experiments, the measured ΔH is a combination of the ΔH of Ca^{2+} binding which primarily involves desolvation of the Ca^{2+} cation and the ΔH of the conformational changes that occur in the protein. However, since the ΔH of Ca^{2+} binding can be approximated to be zero (*31* and references therein), we can assume that the ΔH measured for binding of Ca^{2+} to CIB is nearly entirely derived from the conformational changes that occur in the protein. Therefore, the considerably larger ΔH for binding of Ca^{2+} to EF-4 (−32.4 ± 6.91 kcal/mol) compared to that for binding to EF-3 (−6.22 ± 1.22 kcal/mol) is consistent with the greater conformational change observed in our NMR data. In contrast to Ca^{2+} binding, only one Mg^{2+} ion was found to bind to CIB with considerably lower affinity ($K_d \sim 120$ μM), justifying the complete displacement of Mg^{2+} for Ca^{2+} in EF-3 observed in our NMR data. Although our NMR results suggested that binding of Mg^{2+} to apo-CIB induces a conformational change which is similar in magnitude to that induced by Ca^{2+} binding, the ΔH of Mg^{2+} binding (−8.64 ± 0.49 kcal/mol) was found to be significantly lower. Interestingly, binding of Mg^{2+} to proteins is typically endothermic (*31*, *32*). Also, the interactions of Ca^{2+} with EDTA ($\Delta H = -6.3$ kcal/mol) and Mg^{2+} with EDTA (4.5 kcal/mol), measured under identical conditions, are distinct (results not shown). Therefore, we suggest that the measured ΔH for binding of Mg^{2+} to apo-CIB in these experiments arises from enthalpic cancellation between an endothermic and an exothermic component, for Mg^{2+} binding and the conformational change, respectively.

The binding of Ca^{2+} to EF-3 in the presence of saturating Mg^{2+} concentrations gave a similar K_d (0.48 ± 0.03 μM) for the binding in the absence of Mg^{2+}, indicating that Mg^{2+} does not alter the Ca^{2+} binding affinity of this site (Table 1). However, the ΔH of binding was nearly 80% lower in the presence of Mg^{2+}, most likely because the Mg^{2+}-bound protein is already considerably more folded than apo-CIB. Interestingly, the calculated K_d for binding of Ca^{2+} to EF-4 (198 μM) was ~100-fold lower than in the absence of Mg^{2+},

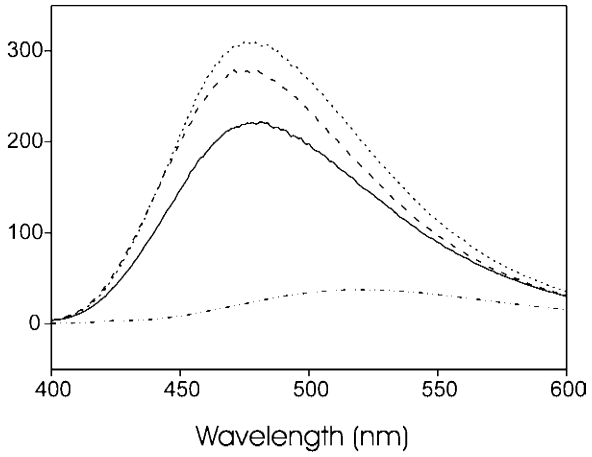

FIGURE 5: Fluorescence spectra of the hydrophobic probe ANS used to monitor the exposed hydrophobic surface area of apo-CIB (- - -), Ca−CIB (—), Mg−CIB (···), and ANS in the absence of CIB (-··-). The *y*-axis represents the fluorescence intensity in arbitrary units.

even though our NMR data demonstrated that Ca^{2+} bound to this site with high affinity (Figure 3G,H). This apparently weak affinity is likely due primarily to enthalpic cancellation during the Ca^{2+} for Mg^{2+} exchange and not from an actual lowering of the Ca^{2+} affinity of this site. Similarly, the affinity of EDTA for Ca^{2+} was found to decrease by nearly 1000-fold in the presence of Mg^{2+} as calculated from ITC titrations performed under our experimental conditions (results not shown). Agah and co-workers also reported a similar trend in the presence of 150 mM NaCl (*32*). Because of this effect, the data for binding of Ca^{2+} to EF-4 are much better resolved, thereby giving a stoichiometry of binding which is closer to the expected 1.0 equiv (0.66 ± 0.00). This also suggests that there is likely ~0.3 equiv of residual Ca^{2+} initially bound to CIB which we were unable to remove with Calcium Sponge S. Titration of Mg^{2+} into a sample of Ca−CIB proceeded with essentially no heat changes in comparison to the control, confirming that Mg^{2+} does not displace Ca^{2+} from EF-3.

ANS Fluorescence Spectroscopy. The metal-free forms of typical regulatory EF-hand calcium-binding proteins, including CaM and recoverin, are well-folded with their hydrophobic residues buried within the protein interior. Therefore, they display very weak fluorescence in the presence of hydrophobic fluorescent probes such as ANS. Subsequent Ca^{2+} binding causes the opening of hydrophobic patches on the protein surface which interact with target proteins or hydrophobic probes, resulting in considerable increases in their fluorescent intensity (*33*−*36*). We recorded ANS fluorescence spectra in the presence of apo-, Ca−, and Mg−CIB. As shown in Figure 5, we found significant ANS fluorescence in the presence of all three forms of CIB, indicating that they all have exposed hydrophobic residues. Interestingly, the intensity was the lowest for Ca−CIB, and the highest for Mg−CIB, with the apo-CIB sample producing an intermediate fluorescent signal, although closer in intensity to that of Mg−CIB. The results are consistent with apo-CIB existing in a molten globule state with some exposed hydrophobic residues. They also suggest that Ca−CIB has an exposed hydrophobic surface area which might be important for its interaction with $\alpha IIb\beta_3$, as has been previously suggested (*3*). The possibility that Mg−CIB may also have an exposed hydrophobic binding patch which might interact with $\alpha IIb\beta_3$ is also intriguing.

DISCUSSION

In this study, we have used a variety of experimental techniques to demonstrate that CIB can specifically bind both Ca^{2+} and Mg^{2+}, and in doing so, these metal ions induce conformational changes in the protein. However, the mechanism, stoichiometry, and affinity of binding as well as the conformational changes that binding induces differ between the two ions. Interestingly, two Ca^{2+} ions were found to sequentially bind to CIB with K_d values near 0.54 and 1.9 μM for binding to EF-4 and EF-3, respectively. The K_d for EF-4 was unchanged in the presence of Mg^{2+}, and although an accurate K_d could not be obtained for EF-3, the interaction was found to remain sequential under these conditions. The sequential nature of this interaction was unexpected since the majority of EF-hand pairs such as those of CaM fold into a tightly associated domain structure, and cooperatively bind to Ca^{2+} (*37*−*39*). Sequential Ca^{2+} binding is typically observed only in proteins such as recoverin (*40*), Frq1 (*21*), and calerythrin (*29*), which have Ca^{2+}-binding sites in different domains. Interestingly, this different Ca^{2+} affinity found with CIB may allow the protein to respond to a greater range of intracellular Ca^{2+} concentrations than if the interaction were to be cooperative.

Another characteristic of CIB that is not observed with many other Ca^{2+}-binding proteins is the ability to specifically bind Mg^{2+}. However, our results indicated that only a single Mg^{2+} ion binds to CIB with physiologically relevant affinity (~120 μM), and it binds to the site that had the lower Ca^{2+} affinity, EF-3. This behavior differs from that of proteins such as troponin C (TnC) which binds Mg^{2+} ions with its high-affinity Ca^{2+} and Mg^{2+} sites that have a higher affinity for Ca^{2+} and does not bind Mg^{2+} with its lower-affinity Ca^{2+}-specific sites (*41*−*43*). Since the intracellular Mg^{2+} concentration (10^{-3} M) is approximately 10^4-fold higher than that of Ca^{2+} (10^{-7} M) (*44*), our results suggest that in the absence of an intracellular Ca^{2+} stimulus the predominant form of CIB within the cell would be Mg_1−CIB. Then, in response to stimulus-induced increasing Ca^{2+} concentrations, Mg_1−Ca_1−CIB and ultimately Ca_2−CIB become the major intracellular forms of the protein, providing three unique metal ion-bound states of the protein that may each have unique functional properties.

Several studies suggest that the biochemical basis for these different Ca^{2+} and Mg^{2+} binding affinities may simply lie in the slightly different Ca^{2+}-binding loop sequences of EF-3 and EF-4 of CIB (*45*−*47*). While the Ca^{2+} chelating residues at positions *X*, *Y*, *Z*, −*X*, and −*Y* as well as the Gly6 residue are all conserved between the two loops, the important chelating residue at the −*Z* position is an Asp in EF-3 and a Glu in EF-4 (*1*). Comparison of the loop sequences of more than 500 different EF-hands from various proteins has revealed that a Glu at this position is highly favored (92%) over an Asp side chain (8%), suggesting that a Glu for Asp substitution may have some functional consequences (*48*). In fact, mutational studies with the smooth muscle myosin regulatory light chain (RLC) and parvalbumin have demonstrated that the presence of a Glu residue at position −*Z* produces a loop which is highly Ca^{2+}-specific with high

affinity, whereas an Asp residue at this position produces a Ca^{2+} and Mg^{2+} binding site with lower Ca^{2+} affinity than the loop containing Glu, but higher Ca^{2+} affinity than Mg^{2+} affinity (*45*−*47*). On the basis of these results, it seems reasonable to suggest that the ability of EF-3 to bind Mg^{2+} may simply result from the substitution of Asp for Glu at the $-Z$ position of the loop sequence. However, we should note that there are some Ca^{2+}-binding loops that do contain Glu residues at the $-Z$ position that also bind Mg^{2+} (*49*−*51*), suggesting that other residues within the sequence may also be important.

Our characterization of the Ca^{2+}-, Mg^{2+}-, and metal-free states of CIB has suggested that binding of both Ca^{2+} and Mg^{2+} to CIB provides the protein with important structural stability. While we found that apo-CIB did have some secondary and tertiary structure by CD spectroscopy, our DSC and NMR experiments suggested that the protein likely adopts a highly flexible and perhaps molten globule type of conformation. A dynamic molten globule structure is also consistent with the considerable amount of hydrophobic surface area observed in our ANS fluorescence results, as well as with the larger hydrodynamic radius we have previously calculated for apo-CIB using pulse field gradient diffusion NMR spectroscopy (*52*), although these values may also be affected by aggregation. Similar types of structures and aggregation properties have also been observed for several related Ca^{2+}-binding proteins such as calerythrin (*29*), Frq1 (*21*), and GCAP-2 (*20*) as well as the unrelated Ca^{2+}-binding proteins α-lactalbumin and lysozyme (*53* and references therein), suggesting that this type of dynamic structure is not unique to apo-CIB. As in CIB, binding of Ca^{2+} to these proteins induced conformational changes which resulted in structural stabilization and similar improvements in NMR spectra. Therefore, a molten globule-like apo form and a well-folded Ca^{2+}-bound structure appear to be common features of many Ca^{2+}-binding proteins.

The Ca^{2+}-induced conformational changes in CIB observed in this study provide a structural basis for the increased affinity of CIB for the cytoplasmic domain tail of the αIIb subunit of platelet integrin $\alpha IIb\beta_3$ in the presence of Ca^{2+} (*1*, *3*−*5*). However, several studies have suggested that an interaction between CIB and αIIb also occurs in the absence of Ca^{2+}, albeit with considerably reduced affinity (*3*, *5*; A. P. Yamniuk and H. J. Vogel, unpublished observations). This is interesting because regulatory EF-hand Ca^{2+}-binding proteins change from a "closed" apo conformation to an "open" Ca^{2+}-bound structure with an exposed hydrophobic binding patch that interacts with hydrophobic regions on the target protein. Unlike many other Ca^{2+}-binding proteins, our ANS fluorescence studies suggested that apo-CIB also has a significant amount of exposed hydrophobic surface area. Interestingly, the recoverin homologue GCAP-2 exhibited similar ANS fluorescence properties with more intense fluorescence in the absence than in the presence of Ca^{2+} (*54*), and this protein also exhibited similar NMR spectra in the Ca^{2+}-free form (*20*). Although to our knowledge there are no published data on an interaction between CIB and αIIb in the presence of Mg^{2+}, the large hydrophobic surface area displayed in our ANS fluorescence results together with the similarities in Ca−CIB and Mg−CIB structures observed in our NMR results suggests that Mg−CIB may also be capable of binding to αIIb. Similar behavior has also been observed with TnC where binding of Mg^{2+} to some of its Ca^{2+}-binding sites is essential for structural stabilization and interaction with its target protein in the absence of Ca^{2+} (*41*, *43*, *55*). By analogy to TnC, perhaps Mg−CIB remains constitutively tethered to αIIb, and Ca^{2+} binding is important for triggering integrin activation. The possibility that CIB may be constitutively bound to target proteins is very intriguing since it has been suggested as a possible subunit of Fnk and Snk kinase, playing a role similar to the role CnB plays in the regulation of CnA (*7*−*9*). However, it is also possible that Mg^{2+} binding may simply provide CIB with increased structural stability in the cell. Therefore, the single Glu for Asp substitution at position $-Z$ of EF-3 may provide a simple mechanism for providing structural stability while maintaining the ability to respond to changes in intracellular Ca^{2+} concentrations. Moreover, it has been shown that EF-4 is more important in target protein binding than EF-3 (*5*, *12*).

In conclusion, our studies demonstrate that both Ca^{2+} and Mg^{2+} can specifically bind to CIB with different stoichiometries and affinities, but each induces conformational changes which stabilize the protein from a highly dynamic molten globule conformation in the absence of bound metal ion to a highly α-helical well-folded globular protein. However, the Mg^{2+}-induced conformational changes are slightly less pronounced than those induced by Ca^{2+}, suggesting that the two ions likely provide CIB with unique properties in each case. While the functional consequences of these different binding characteristics and subsequent conformations are currently unknown, structural stabilization and differential target binding and activation properties are two likely possibilities that require further investigation.

ACKNOWLEDGMENT

We thank Drs. Hiroaki Ishida, Aalim Weljie, and Howard Hunter for aid in NMR data acquisition and processing as well as Dr. Deane McIntyre for the upkeep of the NMR spectrometers. The microcalorimetry equipment that was used was funded by the Alberta Network for Proteomics Innovation, which in turn is supported by the Western Economic Diversification program and the Alberta Science and Research Authority (ASRA). The NMR spectrometer that was used was recently upgraded with funds provided by the Canadian Foundation for Innovation, ASRA, and AHFMR. Maintenance of the Bio-NMR center at the University of Calgary is supported by CIHR.

REFERENCES

1. Naik, U. P., Patel, P. M., and Parise, L. V. (1997) Identification of a novel calcium-binding protein that interacts with the integrin alphaIIb cytoplasmic domain, *J. Biol. Chem. 272*, 4651−4654.
2. Vallar, L., Melchior, C., Plancon, S., Drobecq, H., Lippens, G., Regnault, V., and Kieffer, N. (1999) Divalent cations differentially regulate integrin alphaIIb cytoplasmic tail binding to beta3 and to calcium- and integrin-binding protein, *J. Biol. Chem. 274*, 17257−17266.
3. Shock, D. D., Naik, U. P., Brittain, J. E., Alahari, S. K., Sondek, J., and Parise, L. V. (1999) Calcium-dependent properties of CIB binding to the integrin alphaIIb cytoplasmic domain and translocation to the platelet cytoskeleton, *Biochem. J. 342*, 729−735.
4. Barry, W. T., Boudignon-Proudhon, C., Shock, D. D., McFadden, A., Weiss, J. M., Sondek, J., and Parise, L. V. (2002) Molecular basis of CIB binding to the integrin alpha IIb cytoplasmic domain, *J. Biol. Chem. 277*, 28877−28883.

5. Tsuboi, S. (2002) Calcium integrin-binding protein activates platelet integrin alpha IIbbeta 3, *J. Biol. Chem. 277*, 1919−1923.
6. Shattil, S. J., Kashiwagi, H., and Pampori, N. (1998) Integrin signaling: the platelet paradigm, *Blood 91*, 2645−2657.
7. Holtrich, U., Wolf, G., Yuan, J., Bereiter-Hahn, J., Karn, T., Weiler, M., Kauselmann, G., Rehli, M., Andreesen, R., Kaufmann, M., Kuhl, D., and Strebhardt, K. (2000) Adhesion induced expression of the serine/threonine kinase Fnk in human macrophages, *Oncogene 19*, 4832−4839.
8. Kauselmann, G., Weiler, M., Wulff, P., Jessberger, S., Konietzko, U., Scafidi, J., Staubli, U., Bereiter-Hahn, J., Strebhardt, K., and Kuhl, D. (1999) The polo-like protein kinases Fnk and Snk associate with a Ca^{2+}- and integrin-binding protein and are regulated dynamically with synaptic plasticity, *EMBO J. 18*, 5528−5539.
9. Ma, S., Liu, M. A., Yuan, Y. L., and Erikson, R. L. (2003) The Serum-Inducible Protein Kinase Snk Is a G(1) Phase Polo-Like Kinase That Is Inhibited by the Calcium- and Integrin-Binding Protein CIB, *Mol. Cancer Res. 1*, 376−384.
10. Ito, A., Uehara, T., and Nomura, Y. (2000) Isolation of Ich-1S (caspase-2S)-binding protein that partially inhibits caspase activity, *FEBS Lett. 470*, 360−364.
11. Stabler, S. M., Ostrowski, L. L., Janicki, S. M., and Monteiro, M. J. (1999) A myristoylated calcium-binding protein that preferentially interacts with the Alzheimer's disease presenilin 2 protein, *J. Cell Biol. 145*, 1277−1292.
12. Fang, X., Chen, C., Wang, Q., Gu, J., and Chi, C. (2001) The interaction of the calcium- and integrin-binding protein (CIBP) with the coagulation factor VIII, *Thromb. Res. 102*, 177−185.
13. Haataja, L., Kaartinen, V., Groffen, J., and Heisterkamp, N. (2002) The small GTPase Rac3 interacts with the integrin-binding protein CIB and promotes integrin alpha(IIb)beta(3)-mediated adhesion and spreading, *J. Biol. Chem. 277*, 8321−8328.
14. Henderson, M. J., Russell, A. J., Hird, S., Munoz, M., Clancy, J. L., Lehrbach, G. M., Calanni, S. T., Jans, D. A., Sutherland, R. L., and Watts, C. K. (2002) EDD, the human hyperplastic discs protein, has a role in progesterone receptor coactivation and potential involvement in DNA damage response, *J. Biol. Chem. 277*, 26468−26478.
15. Hollenbach, A. D., McPherson, C. J., Lagutina, I., and Grosveld, G. (2002) The EF-hand calcium-binding protein calmyrin inhibits the transcriptional and DNA-binding activity of Pax3, *Biochim. Biophys. Acta 1574*, 321−328.
16. Whitehouse, C., Chambers, J., Howe, K., Cobourne, M., Sharpe, P., and Solomon, E. (2002) NBR1 interacts with fasciculation and elongation protein zeta-1 (FEZ1) and calcium and integrin binding protein (CIB) and shows developmentally restricted expression in the neural tube, *Eur. J. Biochem. 269*, 538−545.
17. Hwang, P. M., and Vogel, H. J. (2000) Structures of the platelet calcium- and integrin-binding protein and the alphaIIb-integrin cytoplasmic domain suggest a mechanism for calcium-regulated recognition; homology modelling and NMR studies, *J. Mol. Recognit. 13*, 83−92.
18. Rusnak, F., and Mertz, P. (2000) Calcineurin: form and function, *Physiol. Rev. 80*, 1483−1521.
19. Vogel, H. J. (1994) The Merck Frosst Award Lecture 1994. Calmodulin: a versatile calcium mediator protein, *Biochem. Cell Biol. 72*, 357−376.
20. Ames, J. B., Dizhoor, A. M., Ikura, M., Palczewski, K., and Stryer, L. (1999) Three-dimensional structure of guanylyl cyclase activating protein-2, a calcium-sensitive modulator of photoreceptor guanylyl cyclases, *J. Biol. Chem. 274*, 19329−19337.
21. Ames, J. B., Hendricks, K. B., Strahl, T., Huttner, I. G., Hamasaki, N., and Thorner, J. (2000) Structure and calcium-binding properties of Frq1, a novel calcium sensor in the yeast *Saccharomyces cerevisiae*, *Biochemistry 39*, 12149−12161.
22. Ladant, D. (1995) Calcium and membrane binding properties of bovine neurocalcin delta expressed in *Escherichia coli*, *J. Biol. Chem. 270*, 3179−3185.
23. Kobayashi, M., Takamatsu, K., Saitoh, S., and Noguchi, T. (1993) Myristoylation of hippocalcin is linked to its calcium-dependent membrane association properties, *J. Biol. Chem. 268*, 18898−18904.
24. Ames, J. B., Porumb, T., Tanaka, T., Ikura, M., and Stryer, L. (1995) Amino-terminal myristoylation induces cooperative calcium binding to recoverin, *J. Biol. Chem. 270*, 4526−4533.
25. Flaherty, K. M., Zozulya, S., Stryer, L., and McKay, D. B. (1993) Three-dimensional structure of recoverin, a calcium sensor in vision, *Cell 75*, 709−716.
26. Wishart, D. S., Bigam, C. G., Yao, J., Abildgaard, F., Dyson, H. J., Oldfield, E., Markley, J. L., and Sykes, B. D. (1995) ^{1}H, ^{13}C and ^{15}N chemical shift referencing in biomolecular NMR, *J. Biomol. NMR 6*, 135−140.
27. Sonnichsen, F. D., Van Eyk, J. E., Hodges, R. S., and Sykes, B. D. (1992) Effect of trifluoroethanol on protein secondary structure: an NMR and CD study using a synthetic actin peptide, *Biochemistry 31*, 8790−8798.
28. Strickland, E. H. (1974) Aromatic contributions to circular dichroism spectra of proteins, *CRC Crit. Rev. Biochem. 2*, 113−175.
29. Aitio, H., Laakso, T., Pihlajamaa, T., Torkkeli, M., Kilpelainen, I., Drakenberg, T., Serimaa, R., and Annila, A. (2001) Characterization of apo and partially saturated states of calerythrin, an EF-hand protein from *S. erythraea*: a molten globule when deprived of Ca^{2+}, *Protein Sci. 10*, 74−82.
30. Aramini, J. M., Drakenberg, T., Hiraoki, T., Ke, Y., Nitta, K., and Vogel, H. J. (1992) Calcium-43 NMR studies of calcium-binding lysozymes and α-lactalbumins, *Biochemistry 31*, 6761−6768.
31. Gilli, R., Lafitte, D., Lopez, C., Kilhoffer, M., Makarov, A., Briand, C., and Haiech, J. (1998) Thermodynamic analysis of calcium and magnesium binding to calmodulin, *Biochemistry 37*, 5450−5456.
32. Henzl, M. T., Larson, J. D., and Agah, S. (2003) Estimation of parvalbumin Ca^{2+}- and Mg^{2+}-binding constants by global least-squares analysis of isothermal titration calorimetry data, *Anal. Biochem. 319*, 216−233.
33. Berggard, T., Silow, M., Thulin, E., and Linse, S. (2000) Ca^{2+}- and H^{+}-dependent conformational changes of calbindin D(28k), *Biochemistry 39*, 6864−6873.
34. Cardamone, M., and Puri, N. K. (1992) Spectrofluorimetric assessment of the surface hydrophobicity of proteins, *Biochem. J. 282* (Part 2), 589−593.
35. Hughes, R. E., Brzovic, P. S., Klevit, R. E., and Hurley, J. B. (1995) Calcium-dependent solvation of the myristoyl group of recoverin, *Biochemistry 34*, 11410−11416.
36. LaPorte, D. C., Wierman, B. M., and Storm, D. R. (1980) Calcium-induced exposure of a hydrophobic surface on calmodulin, *Biochemistry 19*, 3814−3819.
37. Andersson, A., Forsen, S., Thulin, E., and Vogel, H. J. (1983) Cadmium-113 nuclear magnetic resonance studies of proteolytic fragments of calmodulin: assignment of strong and weak cation binding sites, *Biochemistry 22*, 2309−2313.
38. Linse, S., Helmersson, A., and Forsen, S. (1991) Calcium binding to calmodulin and its globular domains, *J. Biol. Chem. 266*, 8050−8054.
39. Thulin, E., Andersson, A., Drakenberg, T., Forsen, S., and Vogel, H. J. (1984) Metal ion and drug binding to proteolytic fragments of calmodulin: proteolytic, cadmium-113, and proton nuclear magnetic resonance studies, *Biochemistry 23*, 1862−1870.
40. Permyakov, S. E., Cherskaya, A. M., Senin, I. I., Zargarov, A. A., Shulga-Morskoy, S. V., Alekseev, A. M., Zinchenko, D. V., Lipkin, V. M., Philippov, P. P., Uversky, V. N., and Permyakov, E. A. (2000) Effects of mutations in the calcium-binding sites of recoverin on its calcium affinity: evidence for successive filling of the calcium binding sites, *Protein Eng. 13*, 783−790.
41. Finley, N., Dvoretsky, A., and Rosevear, P. R. (2000) Magnesium−calcium exchange in cardiac troponin C bound to cardiac troponin I, *J. Mol. Cell. Cardiol. 32*, 1439−1446.
42. Szczesna, D., Guzman, G., Miller, T., Zhao, J., Farokhi, K., Ellemberger, H., and Potter, J. D. (1996) The role of the four Ca^{2+} binding sites of troponin C in the regulation of skeletal muscle contraction, *J. Biol. Chem. 271*, 8381−8386.
43. Zot, H. G., and Potter, J. D. (1982) A structural role for the Ca^{2+}-Mg^{2+} sites on troponin C in the regulation of muscle contraction. Preparation and properties of troponin C depleted myofibrils, *J. Biol. Chem. 257*, 7678−7683.
44. Berridge, M. J., Bootman, M. D., and Lipp, P. (1998) Calcium: a life and death signal, *Nature 395*, 645−648.
45. Blumenschein, T. M., and Reinach, F. C. (2000) Analysis of affinity and specificity in an EF-hand site using double mutant cycles, *Biochemistry 39*, 3603−3610.
46. Cates, M. S., Berry, M. B., Ho, E. L., Li, Q., Potter, J. D., and Phillips, G. N., Jr. (1999) Metal-ion affinity and specificity in EF-hand proteins: coordination geometry and domain plasticity in parvalbumin, *Struct. Folding Des. 7*, 1269−1278.
47. da Silva, A. C., Kendrick-Jones, J., and Reinach, F. C. (1995) Determinants of ion specificity on EF-hands sites. Conversion of

the Ca^{2+}/Mg^{2+} site of smooth muscle myosin regulatory light chain into a Ca^{2+}-specific site, *J. Biol. Chem. 270*, 6773−6778.
48. Falke, J. J., Drake, S. K., Hazard, A. L., and Peersen, O. B. (1994) Molecular tuning of ion binding to calcium signaling proteins, *Q. Rev. Biophys. 27*, 219−290.
49. Davis, J. P., Rall, J. A., Reiser, P. J., Smillie, L. B., and Tikunova, S. B. (2002) Engineering competitive magnesium binding into the first EF-hand of skeletal troponin C, *J. Biol. Chem. 277*, 49716−49726.
50. Durussel, I., Mehul, B., Bernard, D., Schmidt, R., and Cox, J. A. (2002) Cation- and peptide-binding properties of human calmodulin-like skin protein, *Biochemistry 41*, 5439−5448.
51. Gopal, B., Swaminathan, C. P., Bhattacharya, S., Bhattacharya, A., Murthy, M. R., and Surolia, A. (1997) Thermodynamics of metal ion binding and denaturation of a calcium binding protein from *Entamoeba histolytica*, *Biochemistry 36*, 10910−10916.
52. Weljie, A. M., Yamniuk, A. P., Yoshino, H., Izumi, Y., and Vogel, H. J. (2003) Protein conformational changes studied by diffusion NMR spectroscopy: application to helix-loop-helix calcium binding proteins, *Protein Sci. 12*, 228−236.
53. Polverino, D. L., Frare, E., Gottardo, R., Van Dael, H., and Fontana, A. (2002) Partly folded states of members of the lysozyme/lactalbumin superfamily: A comparative study by circular dichroism spectroscopy and limited proteolysis, *Protein Sci. 11*, 2932−2946.
54. Gorczyca, W. A., Kobialka, M., Kuropatwa, M., and Kurowska, E. (2003) Ca^{2+} differently affects hydrophobic properties of guanylyl cyclase-activating proteins (GCAPs) and recoverin, *Acta Biochim. Pol. 50*, 367−376.
55. Levine, B. A., Thornton, J. M., Fernandes, R., Kelly, C. M., and Mercola, D. (1978) Comparison of the calcium- and magnesium-induced structural changes of troponin C. A proton magnetic resonance study, *Biochim. Biophys. Acta 535*, 11−24.

BI035432B